Supplement of Atmos. Chem. Phys., 25, 2845–2861, 2025
https://doi.org/10.5194/acp-25-2845-2025-supplement

Atmospheric Chemistry and Physics
Open Access
EGU

Supplement of

Machine learning for improvement of upper-tropospheric relative humidity in ERA5 weather model data

Ziming Wang et al.

Correspondence to: Ziming Wang (ziming.wang@dlr.de)

S1 Evaluation of ERA5 temperature using IAGOS in the UTLS

Simmons et al. (2014) found a temperature uncertainty of 0.1 K near the tropopause in the tropics in the precursor of ERA5 data, the ERA-Interim reanalysis. Figure S1 compares T_{IAGOS} and T_{ERA5} for the same test data set used for further ANN model evaluation (samples from one in every 10 selected days of collected IAGOS waypoints around cruise altitudes between 200 hPa and 400 hPa over eastern Atlantic, western Europe, and Africa in 2020). The classification of clear sky, cloudy, UT, and LS conditions is based only on the current pressure level's *ciwc* and *pv* values. The good agreement between both temperatures is reflected in all tested scenarios - all sky UT, cloudy UTLS, clear sky UTLS, and all sky UT - indicated by high determination coefficients (R^2 of 0.96 - 0.98). The spread of the correlation corresponds to greater variability in T_{IAGOS} when the aircraft flew through clouds or due to the interpolation of the gridded T_{ERA5} to the aircraft's vertical position. The MAE between T_{IAGOS} and T_{ERA5} varies between 0.69 K and 0.80 K across the entire data set. T_{ERA5} has a relatively more obvious cold bias in clear sky UTLS and all sky LS regions, with larger MAE and smaller R^2 values among these four scenarios.

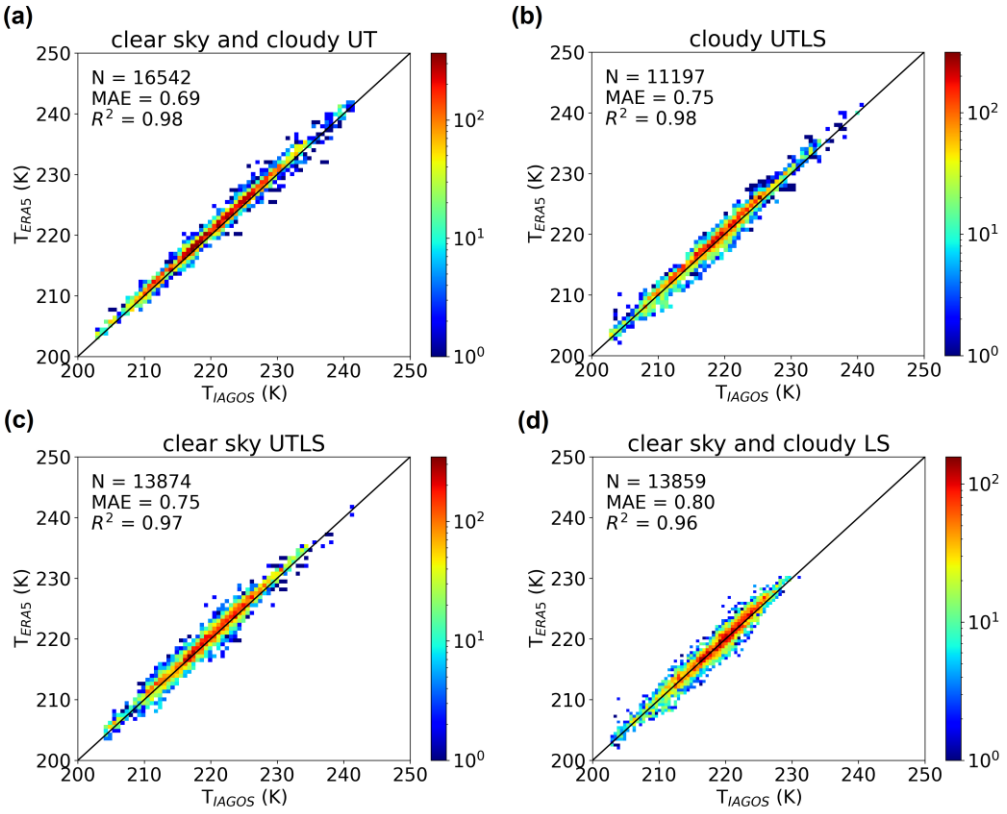

Figure S1: Comparisons of T_{ERA5} against T_{IAGOS} in (a) clear sky and cloudy UT, (b) cloudy UTLS, (c) clear sky UTLS, and (d) clear sky and cloudy LS in the test data set between 200 hPa and 400 hPa over the Atlantic, Europe and Africa for the year 2020.

S2 The correlation between RHi_{IAGOS} and ERA5 temporal meteorological variables

We have determined the temporal dependence of measured RHi_{IAGOS} at the time and location of IAGOS data acquisition on meteorological variables at the preceding time up to 24 hour prior through the calculation of the Pearson correlation coefficient. Based on the calculations, compared to the time 6 hour before, the correlation of RHi_{ERA5} and RHi_{IAGOS} from 0.49 decreases by about 5.4% at the current time. The correlations for T_{ERA5} and z with RHi_{IAGOS} are also statistically significant and almost constant, with coefficients of about -0.5 and 0.4. *w* consistently demonstrates negative correlations with upward motion, resulting in cooling and an increase in RHi. The absolute correlation decreases from the 6-h time lags to the current time from -0.11 by about 86%. The correlation for *u* and *v* tends to fluctuate around 0.34 and 0.44. *d* generally exhibits positive correlations, with the highest value occurring around the 4-h to 5-h time lag, are 0.18 at the 6-h time lag higher than that of

0.03 at the current time by about 83%. In contrast, *vo* continues to exhibit negative correlations with RHi_{IAGOS}, with an increasing absolute correlation coefficient that approaches -0.2.

Including meteorological data from 6 hour prior improves the accuracy of the RHi prediction model on the validation dataset, reducing the MAE from 2.31% to 2.21% and the RMSE from 4.01% to 3.64%. The effect of time lags on model accuracy is calculated and presented in Table S1. As meteorological variables from 1, 2, 3, and 6 hours before the current time are introduced, the decrease in MAE and RMSE gradually becomes more significant. To balance information richness with computational efficiency, we choose the combination of current time, 2 hour, and 6 hour.

Table S1: Impact of including data distributions from 6 hours prior on network prediction accuracy.

Scenarios	MAE (%)	RMSE (%)	R^2
current	2.31	4.01	0.99
current, -1 h	2.21	4.17	0.98
current, -2 h	2.3	4.01	0.98
current, -3 h	2.33	4.01	0.98
current, -6 h	2.21	3.64	0.98
current, -2h, -6h	2.23	3.78	0.99

S3 Preparation of training and validation data

Accounting for the typical time spans of water vapor transport mechanisms, including deep convection, warm conveyor belt uplift regimes, and slow ascending flows, the criteria for data combination involve a 2-h and 6-h time lag before IAGOS data acquisition, ±2 pressure layers from ERA5, and the current humidity from ERA5 and IAGOS. Subsequently, a data set comprising 4 million samples is compiled for training, validation, and testing.

To ensure model robustness and construct an independent test data set, we now use a sequence-based split: four consecutive days of data are used to build the ANN model, followed by a 1-day gap, with the subsequent day's data reserved for validation or testing. While the primary focus is on improving predictions of higher RHi values and ice supersaturation, the complete range of RHi values supplied to the neural networks enhances the overall accuracy of the model.

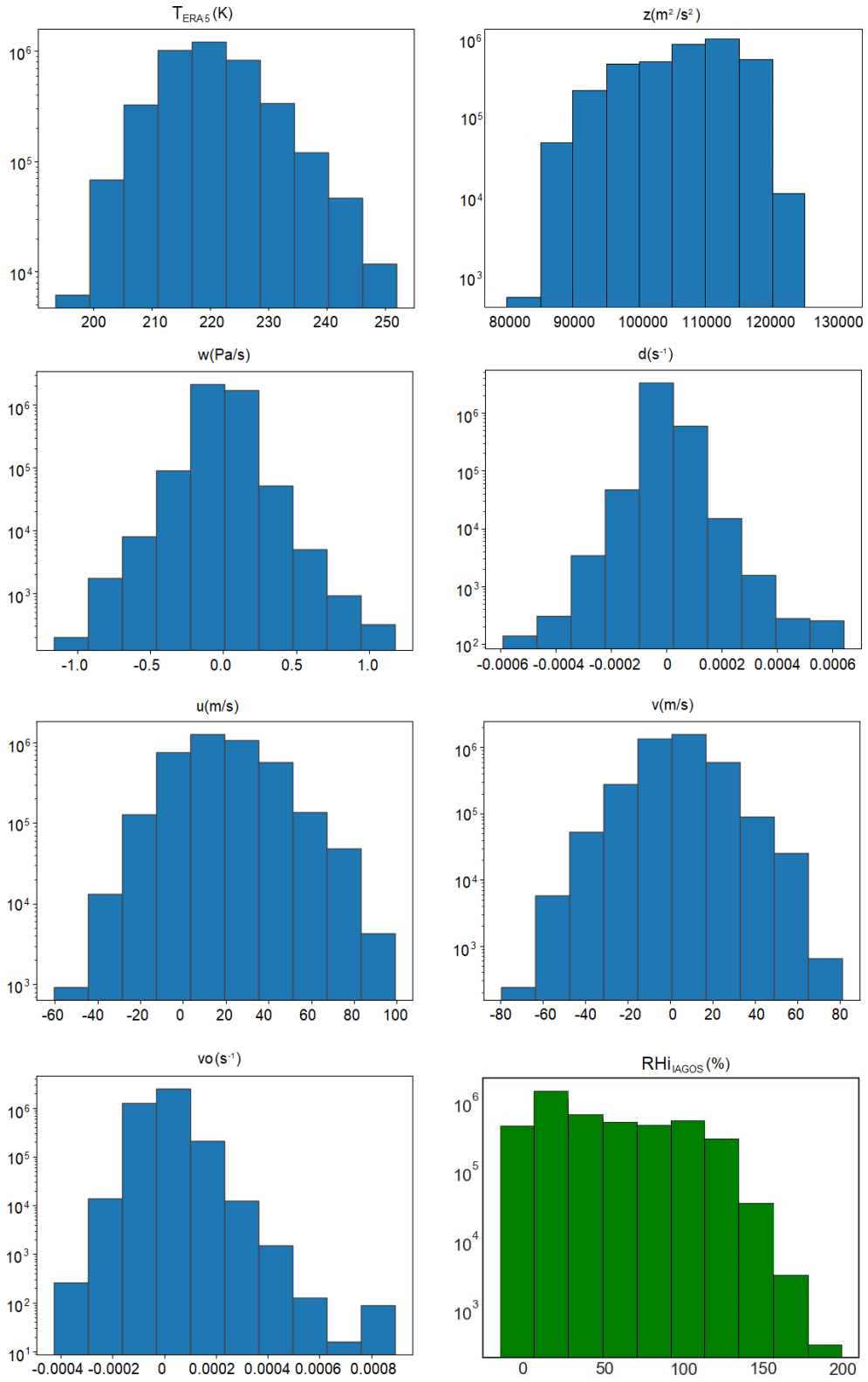

Figure S2: Distributions of input variables including T_{ERA5} (K), z (m^2/s^2), w (Pa/s), d (s^{-1}), u (m/s), v (m/s), and vo (s^{-1}) from ERA5 and valid target RHi_{IAGOS} for the ANN model. The trend of RHi_{ERA5} for the test dataset is shown in Fig. 6.

Distributions of the input and target values in the training data sets are sketched in Fig. S2. Notably, they are not uniformly distributed due to the performed selections as well as the usage of different weather conditions. For instance, T_{ERA5} spans a range from approximately 193 K to 252 K, and the geopotential z encompasses values between roughly 8000 m^2/s^2 and 12500 m^2/s^2. RHi_{IAGOS} values vary across the entire spectrum, ranging from 0 % to 275 %. For the derivation of q_{IAGOS}, the saturation water vapor pressure over ice, p_{ice}, is first calculated using the equation in Murphy and Koop (2005),

$$p_{ice} = e^{(9.550426 - 5723.265/T_{IAGOS} + 3.53968 \ln(T_{IAGOS}) - 0.00728332 T_{IAGOS})} \quad (1)$$

An earlier comparison between different parameterizations of p_{ice} showed that the differences are less than 0.5% for temperatures greater than 173.15 K (Schumann, 2012). In the next step, q is calculated from RHi according to,

$$q = \frac{RHi \times p_{ice} \times R_0}{p \times R_1} \quad (2)$$

where p is the pressure altitude (Pa), R_0 (287.05 $Jkg^{-1}K^{-1}$) and R_1 (461.51 $Jkg^{-1}K^{-1}$) are the real gas constants for air and water vapor, respectively.

S4 Validation of ANN specific humidity in clear and cloudy conditions in the ULTS

q_{ANN} exhibit increased correlations with q_{IAGOS} ($R^2 \geq 0.71$) and decreased bias (MAE $\leq$ 0.06 g/kg) across all scenarios, as evidenced in Fig. S3, when evaluated on its test data set. In the all sky UT (cloudy UTLS) areas, the bias is reduced for q_{ANN} compared to q_{ERA5}, with an increase of R^2 by 0.16/0.12 and a decrease of MAE by 0.03/0.03 g/kg. In the clear UTLS (all sky LS) regimes, the increase of R^2 is 0.16/0.16, and the decrease of MAE is 0.02/0.01 g/kg).

The assessment of specific humidity compared to q_{IAGOS} reveals a greater variability in the results compared to RHi_{ERA5} and RHi_{ANN}. This increased uncertainty can be attributed to biases arising from the transition process between RHi_{IAGOS} and q_{IAGOS}. The presence of 'vertical points' in each plot, deviating from the regression line, indicates limited data points and infrequent measurements under extreme conditions. This, in turn, contributes to the abnormal values in these instances.

The consistency between q_{ANN} and q_{IAGOS} in Fig. S4b is better than that between q_{ERA5} and q_{IAGOS} in Fig. S4a. In Fig. S4c, the MBE of q_{ERA5} compared with q_{IAGOS} is always negative, with the bias increasing up to 0.4 g/kg when q_{IAGOS} reaches 2 g/kg. In Fig. S4d, the ANN model improves the accuracy of q predictions, showing a good agreement for lower water vapor concentrations and an underestimation compared to q_{IAGOS}, which is less pronounced than that of q_{ERA5}.

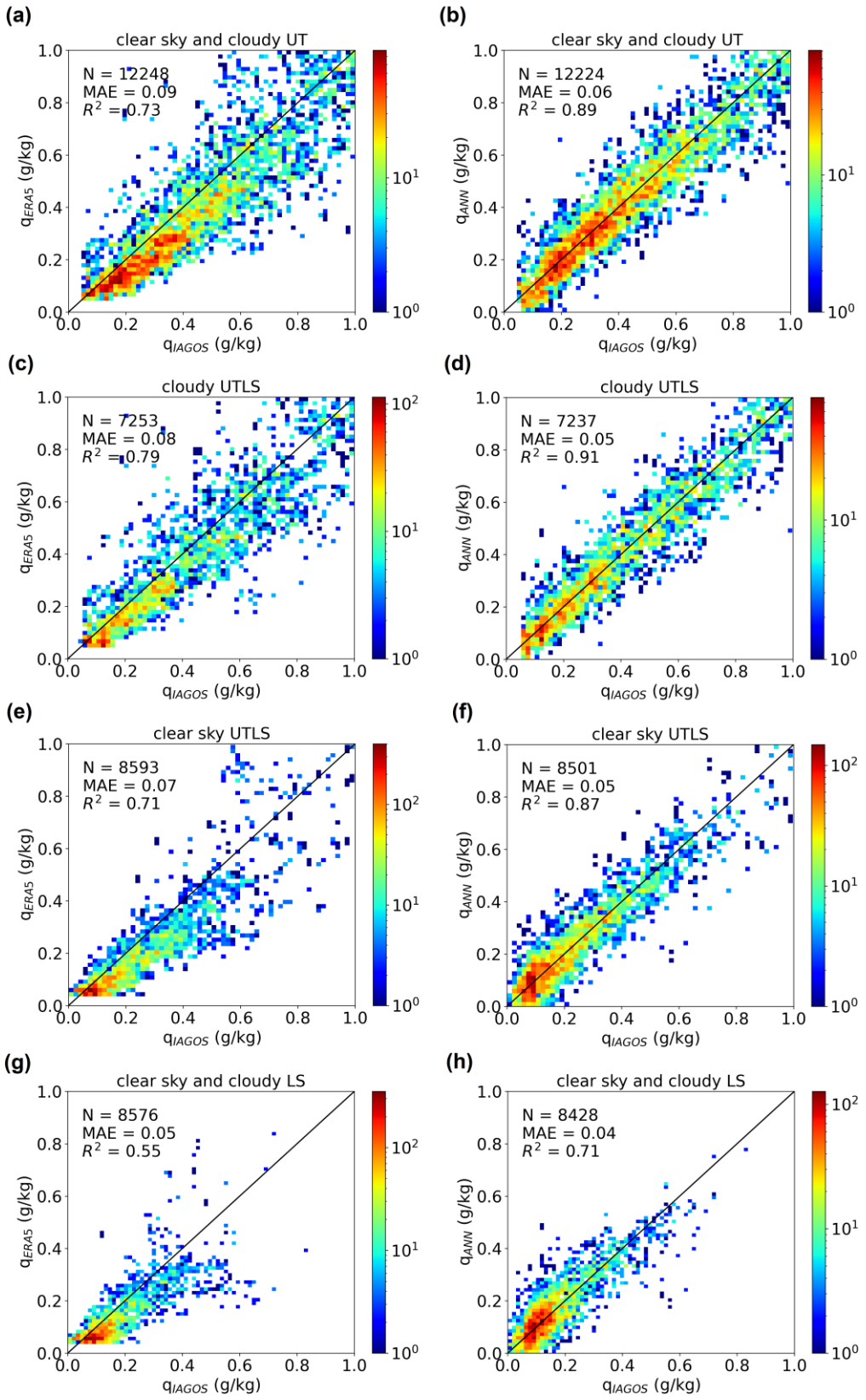

Figure S3: Comparison of q_{ERA5} (left column) and q_{ANN} (right column) against q_{IAGOS} in the (a) and (b) clear sky and cloudy UT, (c) and (d) cloudy UTLS, (e) and (f) clear sky UTLS, and (g) and (h) clear sky and cloudy (or all sky) LS regions in the test data set.

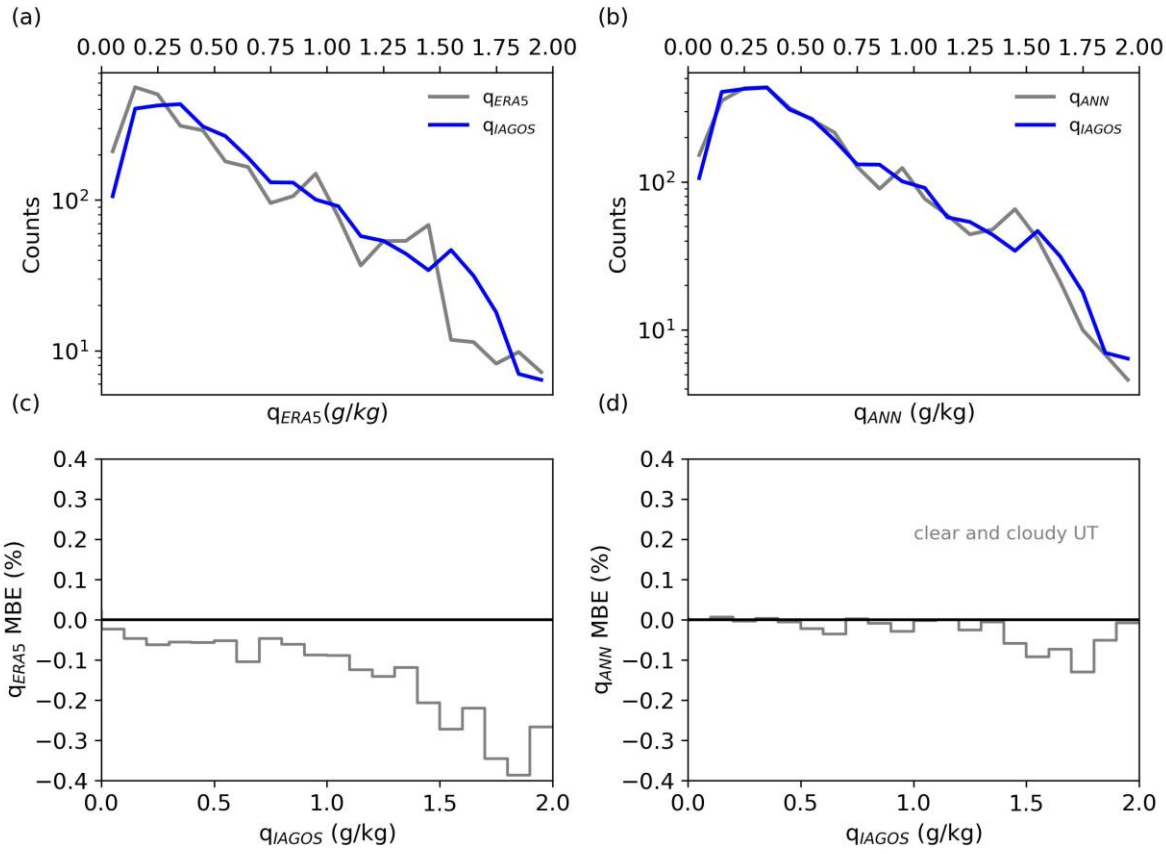

Figure S4: Frequency distribution (a and c) and overall mean biased error MBE (%) (b and d) of q_{ERA5} and q_{ANN} against q_{IAGOS} in the clear sky and cloudy UT (grey) in the test data set.

S5 Comparisons with independent aircraft measurements

The water vapor measurement from AIMS (Atmospheric Ionization Mass Spectrometer) instrument using a backward heated inlet has been evaluated and shown to be in good agreement with other high-quality water vapor data (Kaufmann et al., 2018). Therefore, in addition to the IAGOS measurements, this study uses the independent humidity data records from AIMS (Kaufmann et al., 2016) aboard the HALO aircraft in special weather situations during the CIRRUS-HL campaign to validate the accuracy of RHi prediction from the ANN model.

On 21 July 2021, HALO departed from Germany in the early morning and detected one strong contrail case over the Iberian Peninsula at cruise level. Figure S5 presents RHi_{ERA5} and RHi_{ANN} at 200 hPa at 08:00 UTC on 21 July 2021. It shows that RHi_{ANN} generally reduces RHi in lower pressure regions. Figure S6a and c present RHi_{ERA5} and RHi_{ANN} along the HALO flight track from 06:11 UTC to 09:08 UTC, spanning pressure levels between 146 and 293 hPa, with the flight mainly around 160 hPa. Compared with AIMS measured RHi_{AIMS}, the wet bias of RHi_{ERA5} can reach up to 40% (reddish points) in Fig. S6b. In contrast, the ANN model can reduce the RHi overestimation in the UTLS region within the range of ± 10% (cyan or green points in Fig. S6d).

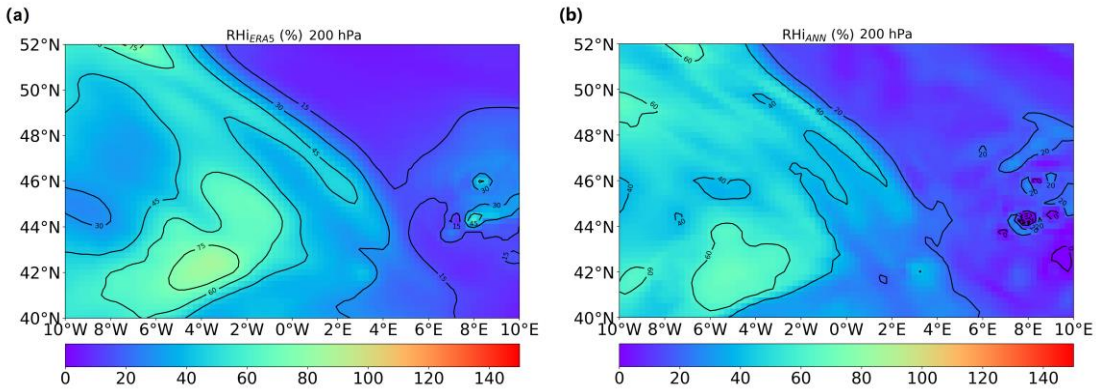

Figure S5: Patterns of (a) RHi_{ERA5} and (b) RHi_{ANN} at 200 hPa at 08:00 UTC on 21 July 2021.

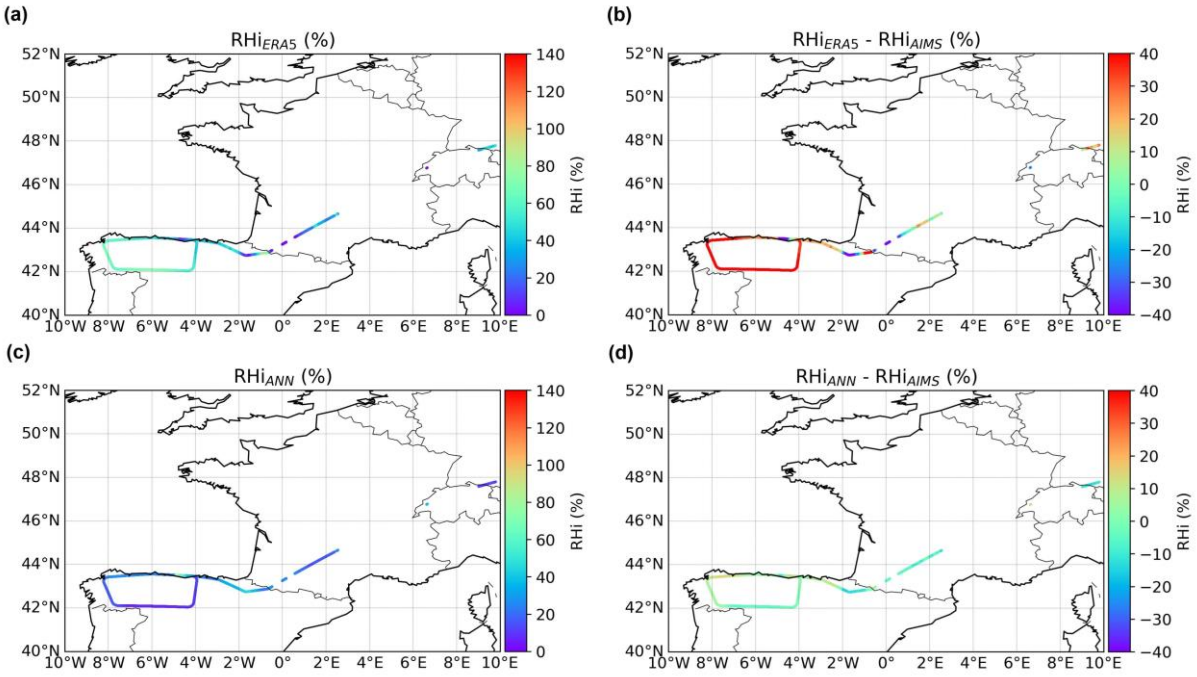

Figure S6: RHi derived from (a) ERA5 or (c) the ANN model and the differences relative to AIMS measurements in (b) and (d) obtained from the HALO aircraft on 21 July 2021 during the CIRRUS-HL campaign. The lines present the HALO flight track.

References

Murphy, D. M. and Koop, T.: Review of the vapour pressures of ice and supercooled water for atmospheric applications, Q. J. Roy. Meteor. Soc., 131, 1539–1565, https://doi.org/10.1256/qj.04.94, 2005.

Schumann, U.: A contrail cirrus prediction model, Geosci. Model Dev., 5, 543–580, https://doi.org/10.5194/gmd-5-543-2012, 2012.

Simmons, A. J., Poli, P., Dee, D. P., Berrisford, P., Hersbach, H., Kobayashi, S., and Peubey, C.: Estimating low-frequency variability and trends in atmospheric temperature using ERA-Interim, Q. J. Roy. Meteor. Soc., 140, 329–353, https://doi.org/10.1002/qj.2317, 2014.